Biochem. J. (2015) **465**, 281–294 (Printed in Great Britain) doi:10.1042/BJ20141045

Protein intrinsic disorder in *Arabidopsis* NAC transcription factors: transcriptional activation by ANAC013 and ANAC046 and their interactions with RCD1

Charlotte O'Shea*, Mikael Kryger*, Emil G. P. Stender*, Birthe B. Kragelund*, Martin Willemoës* and Karen Skriver*[1]

*Department of Biology, University of Copenhagen, 5 Ole Maaloesvej, Copenhagen DK-2200, Denmark

Protein ID (intrinsic disorder) plays a significant, yet relatively unexplored role in transcription factors (TFs). In the present paper, analysis of the transcription regulatory domains (TRDs) of six phylogenetically representative, plant-specific NAC [no apical meristem, ATAF (*Arabidopsis* transcription activation factor), cup-shaped cotyledon] TFs shows that the domains are present in similar average pre-molten or molten globule-like states, but have different patterns of order/disorder and MoRFs (molecular recognition features). ANAC046 (*Arabidopsis* NAC 046) was selected for further studies because of its simple MoRF pattern and its ability to interact with RCD1 (radical-induced cell death 1). Experiments in yeast and thermodynamic characterization suggest that its single MoRF region is sufficient for both transcriptional activation and interaction with RCD1. The remainder of the large regulatory domain is unlikely to contribute to the interaction, since the domain and truncations thereof have similar affinities for RCD1, which are also similar for ANAC013–RCD1 interactions. However, different enthalpic and entropic contributions to binding were revealed for ANAC046 and ANAC013, suggestive of differences in binding mechanisms. Although substitution of both hydrophobic and acidic residues of the ANAC046 MoRF region abolished binding, substitution of other residues, even with α-helix-breaking proline, was less disruptive. Together, the biophysical analyses suggest that RCD1–ANAC046 complex formation does not involve folding-upon-binding, but rather fuzziness or an unknown structure in ANAC046. We suggest that the ANAC046 regulatory domain functions as an entropic chain with a terminal hot spot interacting with RCD1. RCD1, a cellular hub, may be able to interact with many different TFs by exploiting their ID-based flexibility, as demonstrated for its interactions with ANAC046 and ANAC013.

Key words: intrinsic disorder, molecular recognition feature (MoRF), NAC transcription factor, radical-induced cell death 1 (RCD1), transcription regulatory domain, thermodynamics of interaction.

INTRODUCTION

Within the last decade it has become apparent that proteins or protein regions can be intrinsically disordered, meaning that they do not adopt well-defined structures, but instead constitute dynamic ensembles of conformers [1], still with essential functions [2,3]. About one-third of eukaryotic proteins contain regions of more than 30 residues with ID (intrinsic disorder) [4], which results in extraordinary flexibility and, therefore, a large interaction potential. ID regions may fold-upon-binding [5], but additional mechanisms and features have been suggested for their interactions. These include MoRFs (molecular recognition features), which are short, loosely-structured regions forming local structure upon binding [6], preformed structural elements, which form structures with substantial stability in an ID region and persist in complexes [7] and conserved sequence motifs referred to as linear motifs [8]. The interactions of linear motifs are typically weak, transient and possibly of limited specificity. However, both affinity and specificity may increase by cooperative interaction between linear motifs and flanking regions, including longer disordered domains or additional motifs [9,10]. Upon interaction, ID regions lose conformational flexibility, resulting in an entropic cost [11] which may be compensated by a gain in enthalpy. Control of entropy has been suggested to be important for tuning the function of ID regions [11], making determination of the relative contribution of entropy and enthalpy to ID-based interactions highly relevant. Isothermal titration calorimetry (ITC) represents an obvious method for determination of these parameters [12].

Many of the functions associated with long ID regions are related to regulation via translation and transcription and the degree of predicted disorder of the TRDs (transcription regulatory domains) of TFs (transcription factors) is extremely high (73 %–95 %) [13]. Regulation of TFs is essential and takes place through protein–protein interactions, post-translational modifications and alternative splicing [3]. For example, the disordered TRD of the tumour suppressor p53 contains many phosphorylation sites and its affinity for its co-activator is proportional to the number of phosphoryl groups in the TRD [14]. Although the DBDs (DNA-binding domains) of TFs are mostly structured, remote ID regions may also influence both the specificity and affinity of DNA-binding by interacting with the DNA-binding surface. These interactions are characterized by fuzziness, referring to various

Abbreviations: ABA, abscisic acid; ANAC, *Arabidopsis* NAC; AP2, APETALA2; CaM, calmodulin; CD, circular dicroism; Col-0, Columbia ecotype 0; DAS, days after sowing; DBD, DNA-binding domain; DREB2a, AP2/ERF TF, dehydration-responsive element binding protein 2a; ERF, ethylene responsive factor; *Hv*NAC, *Hordeum vulgare* NAC domain containing protein; *Hv*RCD1, *Hordeum vulgare* radical-induced cell death 1; ID, intrinsic disorder; ITC, isothermal titration calorimetry; MEME, multiple EM (expectation maximization) for motif elicitation; MoRF, molecular recognition feature; MS, Murashige and Skoog; NAC, no apical meristem, *Arabidopsis* transcription activation factor, cup-shaped cotyledon; RCD1, radical-induced cell death 1; RT, reverse transcription; SA, salicylic acid; SOG1, suppressor of γ response 1; TF, transcription factor; TFE, trifluoroethanol; TMAO, trimethylamine *N*-oxide; TRD: transcription regulatory domain.

[1] To whom correspondence should be addressed (email kskriver@bio.ku.dk).

degrees of disorder [15]. Such ID-based allosteric regulation may generally involve changes in conformation, flexibility and spacing within a complex, but also competition for binding [16,17]. Recent studies have demonstrated an expanded functional repertoire of ID proteins, compared with structured protein, in their ability to reverse the effect of a particular signal [18]. This ability was explained by the structural heterogeneity of ID as ensembles of conformers that can become redistributed differently upon perturbation [19]. These examples demonstrate the enormous functional potency of ID proteins.

Although the *Arabidopsis thaliana* proteome was predicted to be less disordered than the human proteome, some of the biological processes mediating environmental stimuli are enriched in ID in *Arabidopsis*. This includes processes involved in the perception of light, abiotic stress responses and protein chaperoning [20,21] and may reflect the power of ID in processes requiring rapid and extensive wiring of molecular networks in response to environmental cues [20]. Several years ago it was suggested that phosphorylation is involved in control of *in vivo* stability and activity of the ID region of the bZIP (basic leucine zipper) TF long hypocotyl 5 [22,23], which promotes photomorphogenic development. Additional plant TFs harbour large ID regions [24]. Thus, DREB2a [AP2/ERF (APETALA2/ethylene responsive factor) TF, dehydration-responsive element binding protein 2a], which functions in abiotic stress responses, has a long C-terminus which lacks secondary structure. Interactions between DREB2a and the mediator subunit, Med25, which resulted in gain of structure, possibly in DREB2a [25] and a linear motif which lies in a region with α-helical propensity [26] within the ID region of DREB2a [24,25], mediated interactions with the cellular hub radical-induced cell death 1 (RCD1) [27]. RCD1 plays multiple roles in hormone signalling, responses to reactive oxygen species and development [28]. As a cellular hub, RCD1 interacts with TFs from several different families [27], although no common RCD1-binding site or motif has been identified [24,26]. It was suggested that RCD1 exploits the flexibility of ID in the TFs for the interactions, emphasizing the importance of ID to an integrative hub node in signalling networks [24]. Since knockouts of both *rcd1* and several of its interacting *tf*s are associated with phenotypic changes, the RCD1–TF system represents a model for analysis of ID-based interactions, also *in vivo* [24].

The RCD1 interaction network also includes three members, *Arabidopsis* NAC [no apical meristem, ATAF (*Arabidopsis* transcription activation factor), cup-shaped cotyledon] domain containing protein ANAC013, ANAC046 and ANAC082, of the NAC TF family. This plant-specific protein family contains more than a 100 genes [29] and members of the family play important roles in development, senescence and stress responses [30–33]. Their functional importance and applied potential is highlighted by the effects of over-expression or knockout of specific genes, which can result in improved drought tolerance [34] or delayed senescence, as in the case of *NAP* (NAC-like, activated by AP3/PI), which is a likely positive regulator of senescence [32]. Among the RCD1-interacting NAC TFs, ANC046 and ANAC013 have also been associated with senescence [35]. ANAC013, predicted to be membrane-bound, was recently shown to function in mitochondrial retrograde regulation of oxidative stress responses [36]. Consistent with the structural modularity of TFs, NAC TFs consist of a conserved N-terminal DBD, the NAC domain and diverse C-terminal TRDs [29]. The tertiary structure has been determined for the conserved NAC domain from *Arabidopsis* ANAC019 [37] and rice SNAC1 (stress-responsive NAC1) [38]. The folds of the two domains are similar and consist of a seven-stranded antiparallel twisted β-sheet flanked by an α-helical element on either side of the sheet. The TRDs, predicted to be disordered, contain sub-group-specific linear motifs dominated by polar and charged residues, but with highly conserved hydrophobic or aromatic residues embedded in the polar matrix [29]. The C-terminal regions of *Hordeum vulgare* (barley) *Hv*NAC005 (*Hordeum vulgare* NAC domain containing protein 5) and *Hv*NAC013 have been shown by biophysical and biochemical analyses to be mostly disordered. Surprisingly, no secondary structure induction was detected upon interaction between the *Hv*NAC013 ID region and *Hv*RCD1 (*Hordeum vulgare* radical-induced cell death 1) [39]. In this present work, we present a systematic *in silico* analysis of NAC TRD ID and use the analysis as a platform for thermodynamic characterization of the NAC ID-based interactions with RCD1 to improve understanding of the interaction mechanism of a small folded hub protein and its disordered interaction partners.

EXPERIMENTAL

Bioinformatical analysis

The name and accession numbers of the NAC TFs analysed in this study are: ANAC019, At1g52890; ATAF1 (ANAC002), At1g01720; SOG1 (suppressor of γ response 1; ANAC008), At1g25580; NAP (ANAC029), At1g69490; ANAC013, At1g32870; ANAC046, At3g04060; NTL8 [NTM1 (NAC with transmembrane motif(1)-like8] (ANAC040), At2g27300. ID was predicted using DISOPRED and secondary structure was predicted using PSIPRED [40]. MoRFs were predicted using MoRFpred [41] and sequence motifs were predicted using MEME [multiple EM (expectation maximization) for motif elicitation] [42]. Alignments and the phylogenetic tree were constructed using ClustalX 2.1 [43]. Microarray data for developmental stages were obtained from the *Arabidopsis* electronic fluorescent pictograph browser at www.bar.utoronto.ca using ATH1 microarray samples (www.arabidopsis.org). The samples were in triplicate. The data were normalized to the GCOS (GeneChip Operating Software) method, with a target intensity value of 100 (www.bar.utoronto.ca). The signal recorded for a specific gene in each tissue was directly compared with the highest signal recorded. Perturbed ATH1 microarray samples from the Genevestigator data repository (https://www.genevestigator.com/gv/) were analysed for induced expression using a stringent (>2-fold regulation; $P<0.05$) selection criterion. The treatments were: leaves injected with *Pseudomonas syringae* pv. maculicola for 24 h; leaf samples not watered for 7 days; leaf samples treated with 50 mM abscisic acid (ABA) for 3 h; rosette leaf treated with 250 mM NaCl for 24 h; seedlings treated with 2 mM salicylic acid (SA) for 12 h; green tissue treated with 300 mM mannitol for up to 24 h.

Plant materials, growth conditions and quantitative real-time RT-PCR analysis

Arabidopsis Col-0 (Columbia ecotype 0) seeds were surface-sterilized, placed on Murashige and Skoog (MS) agar and stratified for 3 days at 4 °C in the dark. Growth took place for 8 days before seedlings were transferred to 0.5× MS liquid medium and incubated for 16 days. Seedlings were transferred to 0.5× MS liquid medium containing 50 mM ABA for 3 h, 2 mM SA for 12 h or 300 mM mannitol or 250 mM NaCl for 24 h. Plants were grown in controlled environment chambers with a 16-h-light/8-h-dark cycle (120 $\mu Em^{-2} \cdot s^{-1}$) at 22 °C. Plants for senescence studies were transferred from agar to soil and harvested 17 days and 42 days after sowing (DAS). Total RNA was isolated using RNeasy Plant Mini Kit

(Qiagen). Quantitative real-time RT (reverse transcription)-PCR was performed three times on 100 ng of total RNA and 100 ng of primers using Brilliant II SYBR Green QRT-PCR Master Mix Kit (Agilent Technologies). The $2^{-\Delta\Delta CT}$ method was used to calculate relative change in transcript levels [44] with *actin2* as reference to determine relative expression levels. The *ANAC046*-specific primers 5′-GACAACACTTACCTTCCTACCCAA and 5′-TTATTATTGCCTGAACCTGCCC-3′ resulted in an amplicon length of 101 bp and the *actin2*-specific primers 5′-GGTAACATTGTGCTCAGTGGT GG and 5′- AACGACCT-TAATCTTCATGCTGC resulted in an amplicon length of 108 bp.

Production and purification of proteins

Specific primers were used to amplify RCD1 and NAC fragments. The PCR products were inserted into pDEST17 (Invitrogen) or pET15b (Novagen) to obtain histidine-tagged recombinant proteins and pET11a (Novagen) to obtain untagged recombinant proteins. The histidine-tagged NAC proteins were expressed in *Escherischia coli* strain BL21(DE3)pLyS at 37 °C, harvested, resuspended in PBS, 25 % (w/v) sucrose and 1 % (w/v) Triton X-100, treated with DNAse I (10 units/ml) for 15 min and sonicated three times. Soluble histidine–SOG1 (210–449) was purified on TALON resin using standard protocols (Clontech). Insoluble histidine–NTL8 (156–335) was dissolved in 20 mM Tris/HCl, pH 7.5, 4.5 M urea and 0.1 % (v/v) Triton X-100 and centrifuged 10 min at 20000 ***g*** before affinity purification. The untagged recombinant proteins were produced in *E. coli* strain BL21-CodonPlus(DE3)-RP at 37 °C and purified using a denaturation/renaturation procedure for ID proteins as reported previously [39]. The induced cells were harvested, sonicated and resuspended as for histidine–NTL8. The supernatant was applied to a 1-ml Mono Q 5/50 column (GE Healthcare) equilibrated in 20 mM Tris/HCl, pH 7.5, 4.5 M urea and eluted with a linear gradient from 0–1 M NaCl. Subsequently, proteins were dialysed against 50 mM Hepes, pH 7.4, 100 mM NaCl before size-exclusion chromatography on a Superdex™ 75 10/300 GL (gas/liquid) column (GE Healtcare). RCD1–RST (RCD1, SRO, TAF4) (499–572) and histidine–RCD1–RST (487–589) were expressed in BL21-(DE3) at 37 °C, harvested, resuspended in 50 mM NaH_2PO_4/Na_2HPO_4, pH 7.0, 300 mM NaCl, 0.1 % (w/v) Triton X-100, 1 mM PMSF and 1 mM 2-mercaptoehtanol and sonicated. After centrifugation for 20 min at 13000 *g* at 4 °C, the supernatant from expression of RCD1–RST (499–572) was dialysed 3 × 4 h against 20 mM Tris/HCl, pH 8.9, 20 mM NaCl at 4 °C. The sample was centrifuged for 20 min at 4000 *g* and 4 °C before application to a 6 ml cation exchange SOURCE™ 15S column and eluted with a linear NaCl gradient from 20 mM to 1 M NaCl. The supernatant from the histidine–RCD1–RST (487–589) expression was purified on TALON resin (Clontech). Purified proteins were analysed by MALDI–TOF MS (Autoflex Bruker) and SDS/PAGE and dialysed as needed for further analysis.

Analytical size-exclusion chromatography

Analytical size-exclusion chromatography was performed on a Superdex™ 75 10/300 GL column using an Äkta 900 purifier (GE Healthcare). The following proteins were used for calibration: bovine aprotinin (6.5 kDa); cytochrome *c* (12.4 kDa); bovine carbonic anhydrase (29 kDa); BSA (66 kDa). Blue Dextran (2000 kDa) was used for void volume (V_0) determination. Proteins for chromatography were dissolved in 20 mM Tris/HCl, pH 7.0, 150 mM NaCl. DTT was added to a concentration of 10 mM just before protein was loaded on to the column. Stokes radii were calculated according to the method of Uversky [45].

Circular dichroism spectroscopy

Far-UV circular dichroism (CD) spectra were recorded on a Jasco 810 spectropolarimeter at a wavelength range from 250 nm to 190 nm, a scan rate of 10 nm/min, 10 accumulations and 2 s response time. Samples were recorded in a quartz cuvette with a 1-mm path length. For each spectrum, the background buffer spectrum was subtracted and the resulting spectrum smoothed using a Fast Fourier Transform filter (Jasco software). The spectra were obtained for samples containing between 5 μM and 30 μM protein in 10 mM NaH_2PO_4/Na_2HPO_4, pH 7.0. The helicity percentage was estimated using the formula $H = ([\theta]_{222} - 3000)/(-36000 - 3000)$, where $[\theta]_{222}$ is the mean residue ellipticity at 222 nm (in $deg \times cm^2 \times dmol^{-1}$) [46]. When TFE (trifluoroethanol) was included in the experiments, the concentrations ranged from 0 %–40 % (v/v).

Assays in yeast

To detect intrinsic transcriptional activity and protein–protein interaction, ANAC046, ANAC013 and NAP were examined for the presence of an activation domain and for their ability to bind RCD1 using the yeast one- and two-hybrid systems. Full-length or truncated versions of the NAC TF and RCD1 encoding sequences were amplified using sequence specific primers and recombined into the pDEST32/pDEST22 vectors (Invitrogen). ANAC046 mutants were constructed using the QuickChange mutagenesis kit (Stratagene). Plasmids were transformed into yeast strain pJ694A and assayed as described [29].

Isothermal titration calorimetry

ITC was used to determine the thermodynamic parameters K_d and ΔH from which ΔG and ΔS were calculated. The experiments were performed with a MicroCal VP-ITC microcalorimeter (GE Healthcare). Protein samples were dialysed against 50 mM Hepes, pH 7.4 and 100 mM NaCl or as indicated, centrifuged at 15000 *g* for 5 min and degassed for 10 min by stirring under vacuum. Experiments were performed with a concentration of titrand in the sample cell of 3–6 μM and titrator concentrations of 45–90 μM in the syringe. A total of 14 or 28 injections separated by 300 s and with a duration of 20–40 s each of 10–20 μl of titrant was injected into the sample at 25 °C. Data from the ITC experiments were analysed using an Origen 7 software package (MicroCal™) by fitting data to a 'one set of sites' binding model. Standard errors for the thermodynamic parameters ΔH and K_d, as well as the stoichiometry N, were obtained from Origin when fitting the data. The heat of dilution was subtracted from the raw data by performing a titration of titrant against buffer or by subtracting the dilution enthalpy obtained in the last injection when the partial enthalpy change had reached a constant level. Similar results were obtained at least twice for all experiments. N-terminally acetylated and C-terminally amidated peptides were obtained from TAG Copenhagen A/S.

Induced folding of ANAC046 C-terminus

TMAO (trimethylamine *N*-oxide)-induced protein folding was monitored by tryptophan emission fluorescence intensity according to a modified protocol [47]. The concentration of ANAC046 (172–338) was 1 μM in 50 mM Hepes, pH 7.4, 100 mM NaCl and 0–3 M TMAO. TMAO was diluted from a stock solution of 3.5 M TMAO. The samples were mixed,

inverted six times, centrifuged briefly and incubated for 1 h at room temperature before emission scanning from 320–370 nm with scan speed 50 nm/min, excitation slit 7.5 nm, emission slit 10.0 nm and 10 accumulated scans in a PerkinElmer LS55 luminescence spectrometer at 298 K with excitation at 295 nm. Buffer spectra were subtracted from the raw spectra. All samples were prepared in duplicate and measured individually.

The wavelength of the maximum tryptophan emission intensity for a given sample was normalized to:

$$\text{Fraction folded} = \frac{\lambda - \lambda_{\text{unfolded}}}{\lambda_{\text{unfolded}} - \lambda_{\text{unfolded}}} \quad (1)$$

The fraction folded was plotted as a function of the TMAO concentration and by using OriginPro 9.0.0 (64-bit) b45 (Academic) fitted to:

$$\text{Fraction folded} = (\{\text{fraction folded}\}_{\text{F}} + m_{\text{F}}[\text{TMAO}]) + (\{\text{fraction folded}\}_{\text{U}} + m_{\text{U}}[\text{TMAO}]) \times \frac{e^{\frac{\Delta G_{\text{U-F}} - m \times [\text{TMAO}]}{RT}}}{1 + e^{\frac{\Delta G_{\text{U-F}} - m \times [\text{TMAO}]}{RT}}} \quad (2)$$

[48]

RESULTS

NAC ID regions

NAC TFs representing the phylogentic diversity of the *Arabidopsis* NAC family were selected for systematic analysis of the NAC C-termini, hereinafter referred to as TRDs. These included NTL8 [49] of group I, ANAC046 of group II [29], NAP [32] and ANAC019 of group III [29], ANAC013 [36] of group IV and SOG1 [50] of group IX [29] (Figure 1a). In addition to being NAC group representatives, they also play important functional roles. ANAC019 is implicated in abiotic stress responses and functions as a positive regulator of signalling via the plant stress hormone ABA [29]. NTL8, which is membrane-bound, mediates salt regulation of seed germination [49] and SOG1 regulates responses to DNA damage [50]. As mentioned in the introduction, NAP is implicated in senescence [32] and RCD1-interacting ANAC013 is implicated in oxidative stress responses [36]. ANAC046 also interacts with RCD1 [27] and microarray analysis suggests that expression of *ANAC046* is significantly induced during senescence [35] by different stress exposures and by ABA and SA, which are associated with abiotic stress responses and plant defence respectively (Figure 1b). Analysis by quantitative real-time RT-PCR using *ANAC046*-specific primers confirmed the association of *ANAC046* with senescence and stress responses (Figure 1c). The selected NAC TFs all contain a structured N-terminal NAC domain and a mostly disordered C-terminal TRD (Figure 1d). However, their order/disorder patterns are different. For example, the large C-termini of ANAC013 and SOG1 contain several regions of disorder interrupted by short, putatively ordered regions, whereas the NAP TRD was predicted to be completely disordered. Different α-helix and MoRF patterns were also predicted. Whereas only a single and two α-helices were predicted for the ANAC046 and ANAC019 TRDs, respectively, the other TRDs are likely to contain several α-helices. Furthermore, whereas several MoRFs were predicted for ANAC013, ANAC019, SOG1 and NTL8, only a single MoRF, coinciding with the predicted α-helix and, therefore, representing a putative α-MoRF, was revealed for ANAC046.

To analyse the structure and interactions of the TRDs of the six NAC TFs, these regions were produced as recombinant proteins (Figure 2). The complete C-terminal region was produced and purified for ANAC046, NAP and ANAC019, resulting in the recombinant proteins ANAC046 (172–338), NAP (162–268) and ANAC019 (163–317) and ANAC013 was produced without the C-terminal predicted transmembrane α-helix to generate ANAC013 (161–498). For NTL8 and SOG1, an N-terminal histidine-tag was needed to purify soluble protein fragments, named histidine–NTL8 (156–335) and histidine–SOG (210–449), in sufficient amounts. Although the relative migration pattern of the recombinant proteins by SDS/PAGE was in accordance with their relative molecular mass values [NAP (162–268): 15.0 kDa; ANAC019 (163–317): 17.2 kDa; ANAC046 (172–338): 18.2 kDa; histidine–NTL8 (156–335): 20.3 kDa; histidine–SOG (210–449): 29.0 kDa; ANAC013 (161–498): 37.5 kDa], they displayed slow migration during SDS/PAGE compared with standard globular proteins, which is in accordance with their ID nature and previous analysis of two NAC TRDs [39].

Structural analysis of NAC TRDs

Different protein conformational classes (native, molten globule, pre-molten globule and denaturant-unfolded for globular proteins and pre-molten globule-like and coil-like for ID proteins) have characteristic hydrodynamic dimensions and molecular mass correlations [51]. This aspect was analysed by size-exclusion chromatography for the four untagged NAC TRDs. The hydrodynamic radii (Stokes radii) of ANAC046 (172–338), NAP (162–268) and ANAC019 (163–317) corresponded to pre-molten globule states, whereas ANAC013 (161–498) had a more compact structure consistent with its disorder profile (Figures 1d and 3). Since α-helices might exert long-range effects on the structure of ID regions, the putative α-helix region of ANAC046 was removed. No significant structural change was monitored by this truncation to generate ANAC046 (172–318) (Figure 3, inset).

The NAC TRDs were also analysed by CD spectroscopy. Unfolded and disordered proteins have a characteristic far-UV CD spectrum with an intensive minimum near 200 nm and an ellipticity close to zero near 222 nm [52]. ID proteins may be sorted on the basis of $[\theta]222$ (ellipticity) and $[\theta]200$ values into coil-like and pre-molten globule-like sub-classes. Although the spectra of the six recombinant proteins showed different characteristics, they all had a minimum around 200 nm and only slightly negative ellipticities at 222 nm (Figure 4a). Both the $[\theta]222$ and $[\theta]200$ values suggested that histidine–NTL8 (156–335), ANAC013 (161–498), NAP (162–268) and ANAC019 (163–317) are similar, populating pre-molten globule-like ensembles, whereas the values for histidine–SOG1 (210–449) and ANAC046 (172–338) suggest more random coil-like ensembles. The estimated contents of α-helical peptide bonds [46] were close to 20 % for all proteins investigated [25 % for NAP (162–268), 16 % for ANAC046 (172–338), 21 % for ANAC019 (163–317), 16 % for ANAC013 (161–498), 16 % for histidine–SOG1 (210–449) and 16 % for histidine–NTL8 (156–335)].

Induced folding of the ANAC046 TRD

Structure formation in ID proteins is typically studied as a function of solvent conditions [5] and the naturally occurring protective osmolyte TMAO has been used to induce structure in ID regions [47]. The apparently simple ANAC046 TRD was

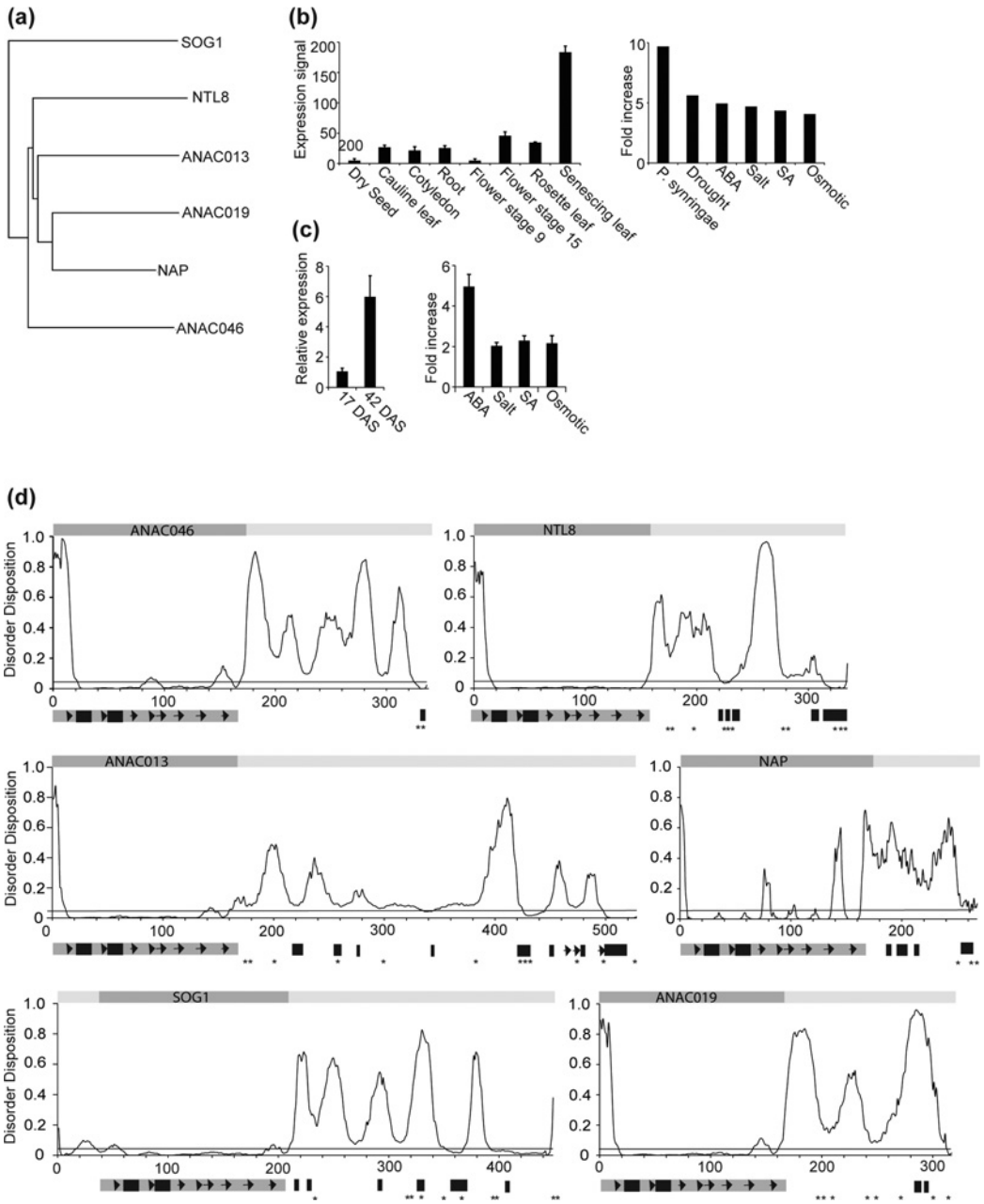

Figure 1 Phylogenetic relationship and predicted structural features of six NAC TFs and ANAC046 expression

(**a**) Phylogenetic relationship of the six NAC TFs analysed in this study. The analysis is based on full-length NAC sequences and alignments and the tree was constructed using ClustalX 2.1 [43]. The accession numbers of the NAC TFs shown are: ANAC019, At1g52890; ATAF1, At1g01720; SOG1, At1g25580; NAP, At1g69490; ANAC013, At1g32870; ANAC046, At3g04060; and NTL8, At2g27300. (**b**) Microarray analysis of *ANAC046* expression. (Left) Microarray data for different developmental stages obtained from the *Arabidopsis* electronic fluorescent pictograph browser (www.bar.utoronto.ca) using ATH1 microarray samples (www.arabidopsis.org). The samples were in triplicate. The signal recorded in each tissue is directly compared with the highest signal recorded for *ANAC046*. (Right) Microarray data for selected hormone, stress and temperature-perturbed ATH1 samples (fold increase compared with control) from the Genevestigator data repository (https://www.genevestigator.com/gv/) were analysed for expression of *ANAC046*. The treatments were: leaf injected with *P. syringae* pv. maculicola; leaf not watered for 7 days; leaf treated with 50 mM ABA for 3 h; rosette leaf treated with 250 mM NaCl for 24 h; seedling treated with 2 mM SA for 12 h; green tissue treated with 300 mM mannitol for up to 24 h. (**c**) Expression of *ANAC046* in *Arabidopsis* Col-0 plants and seedlings. (Left) Relative expression level in plants 17 and 42 DAS. (Right) Seedlings grown in liquid medium were treated with 50 mM ABA for 3 h, 2 mM SA for 12 h or 300 mM mannitol or 250 mM NaCl for 24 h. The values shown are fold increase compared with untreated control seedlings. Values are mean $\pm$ S.D. ($n = 3$). (**d**) DISOPRED disorder prediction [40] for the six NAC TFs. A threshold was applied with disorder assigned to values greater than or equal to 0.05 (black bar). The DNA-binding NAC domains are shown by dark grey bars and the TRDs by light grey bars above the predictions. The approximate positions of α-helices (bars) and β-strands (arrows) predicted by PSIPRED [40] and MoRFs (*) predicted by MoRFpred [41] for the varying TRDs are shown below the disorder predictions. Since the N-terminal NAC folds are very similar, the approximate positions of α-helices (bars) and β-strands (arrows) in the ANAC019 NAC domain [37] (PDB accession code 1UT7) are shown in the lower dark grey bar to represent the NAC domains in all NAC proteins.

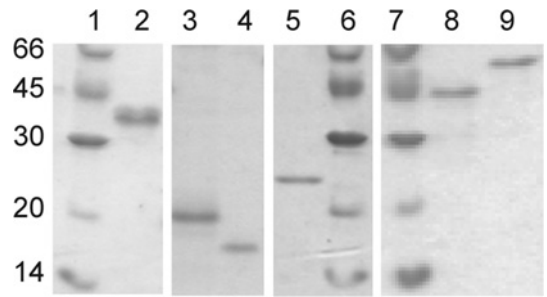

Figure 2 Recombinant NAC TRDs

SDS/PAGE analysis and Coomassie Blue staining of recombinant NAC TRDs. Molecular mass marker with masses in kDa shown at left (lane 1); histidine–NTL8 (156–335; lane 2); ANAC019 (163–317; lane 3); NAP (162–268; lane 4); ANAC046 (172–338; lane 5); histidine–SOG1 (210–449; lane 8); ANAC013 (161–498; lane 9).

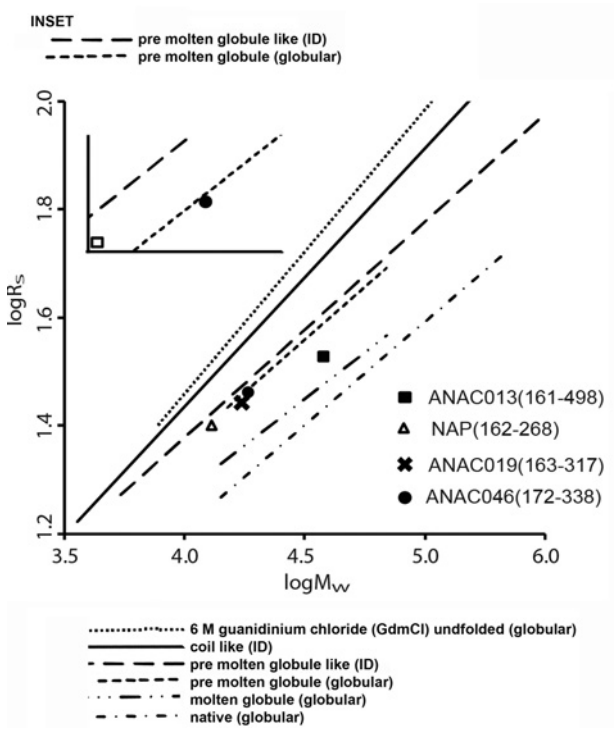

Figure 3 Hydrodynamic volumes of NAC TRDs

Size-exclusion chromatography of the NAC C-termini ANAC046 (172–338), NAP (162–268), ANAC019 (163–317) and ANAC013 (161–498) was performed to determine the Stokes radius and, thereby, average structural state. The trend lines showing the dependence of the hydrodynamic radius (R_S) on the molecular mass for different conformational states is from [51]. Key to the traces has have been removed from the caption and added to the figure, please check.

selected to analyse for structure propensity. ANAC046 (172–338) contains a single tryptophan, Trp^{332}, in the predicted MoRF region (Figure 5) and tryptophan emission was measured using an excitation wavelength of 295 nm. In the absence of TMAO, the maximum emission wavelength λ_{Max} was 355.5 nm (Figure 6, inset), whereas the emission wavelength maximum showed a significant blue shift to 348.5 nm in the presence of 3.0 M TMAO, suggesting that the environment around Trp^{332} became more hydrophobic in the presence of TMAO. The conformational changes were followed by monitoring the wavelength of the maximum fluorescence emission intensities as a function of the TMAO concentration. After fitting (eqn 2) [48], the sigmoid curve observed when plotting the signal maximum wavelength for the various TMAO concentrations resulted in the following values: $R^2 = 0.95$, $\Delta G_{U\text{-}F} = 23.8 \pm 9.6$ kJ/mol, indicative of two-state cooperative folding with burial of the hydrophobic surface of the ANAC046 (172–338).

Transcriptional activity of NAP, ANAC013 and ANAC014

Several studies have shown that the transcription regulatory activity of the NAC TFs resides in the C-terminal regions and is independent of the N-terminal NAC domain [29,39]. For a few NAC TFs, the activity has been mapped to group-specific sequence motifs [39]. This aspect was investigated for NAP, ANAC013 and ANAC046, which were selected for further analysis due to their ability to interact with RCD1 (ANAC013 and ANAC046) and to serve as negative control of the interaction (NAP). Coding regions of the three NAC genes were fused to yeast GAL4 DBD (Figures 7a–7c) and analysed for their ability to activate transcription through the ability to promote selective growth of yeast.

Both full-length NAP and its TRD, NAP (163–268), activated transcription in yeast. MEME motif analysis of the C-terminus revealed only one sequence motif in the TRD, which overlapped with a predicted α-helix (Figures 1d and 7a). Both hydrophobic and charged/polar residues were among the most conserved residues of the motif (Figure 7a). The TRD was truncated from the C-terminus to remove stepwise the predicted MEME motifs, α-helices and MoRFs. This revealed that the ability to activate transcription was retained until the region with the MEME motif was removed, after which no activity was detected. Similar results were obtained from the same C-terminal truncations of full-length NAP, supporting the importance of the MEME motif region for transcriptional activation activity.

Both full-length ANAC013, DBD–ANAC013(1–498) and the TRD, DBD–ANAC013 (161–498), both lacking the transmembrane region, activated transcription in yeast. MEME analyses of the TRD did not reveal any conserved sequence motifs. Stepwise C-terminal truncation of both constructs revealed that removal of the region between residue 205 and 299, containing several MoRFs and α-helices (Figure 1d), abolished the ability to activate transcription (Figure 7b). Interestingly, part of this region resembles the strong EDLL activation motif present in plant AP2/ERF TFs and other acidic activators [53]. Although ANAC013 does not show an exact match (EDLV as opposed to EDLL; Figure 7b), it is a potential candidate as an activating motif.

After demonstrating the ability of full-length ANAC046 and its TRD to activate transcription, analysis of C-terminally truncated versions of these suggested the importance of the MoRF region for the activity (Figure 7c). This was supported by the ability of ANAC046 (315–338) to activate transcription.

Interactions between RCD1 and the ANAC013 and ANAC046 TRDs

Relatively few interactions have been reported between NAC TRDs and other proteins. However, the TRD of *Hv*NAC013 has been shown to interact with the RST domain of *Hv*RCD1 [39], making it likely that ANAC046, a close homologue of *Hv*NAC013, and ANAC013 also use their TRDs for interactions with RCD1 [27]. Yeast two-hybrid assays were initially used to analyse this. As expected, the RST domain of RCD1 interacted with both full-length ANAC013 and ANAC046 and their TRDs (Figures 7b and 7c), whereas no interaction was detected with NAP (Figure 7a) [27]. However, the interaction between

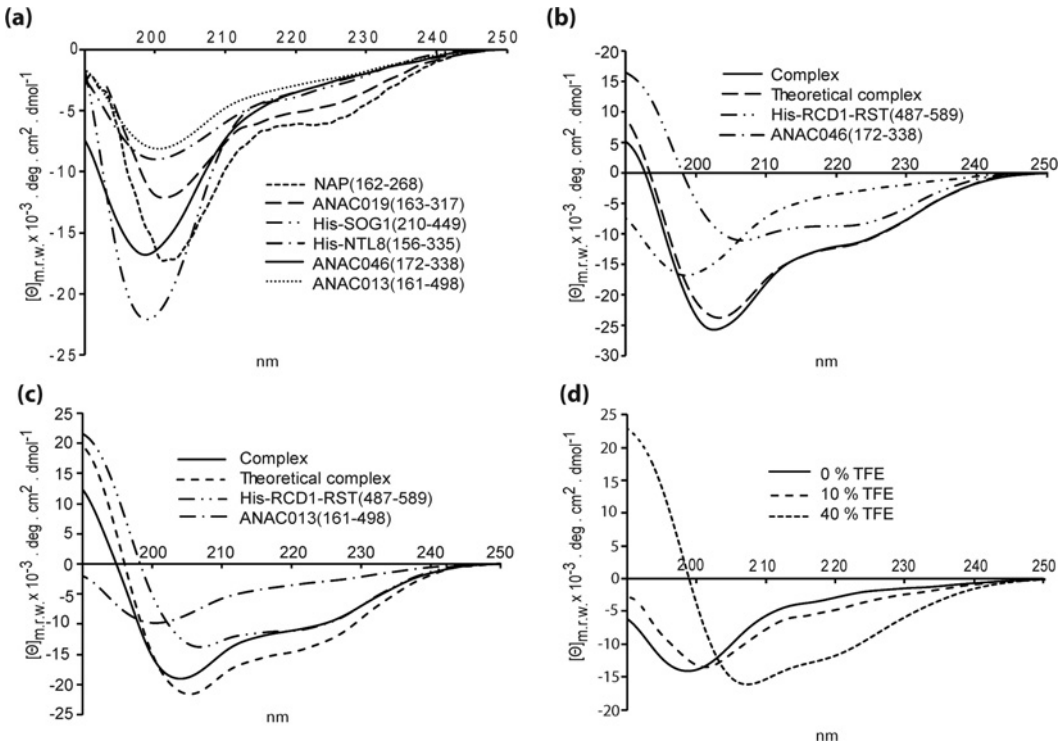

Figure 4 Analysis of NAC TRDs and NAC–RCD1 complexes by CD spectroscopy

(**a**) CD analysis of six NAC TRD structures: NAP (162–268), ANAC019 (163–317), histidine–SOG1 (210–449), histidine–NTL8 (156–335), ANAC046 (172–338) and ANAC013 (161–498). Far-UV CD spectra of 5 μM of NAC TRD in 10 mM Na_2HPO4/NaH_2PO_4, pH 7.0 were recorded and a total of 10 scans were averaged at a wavelength from 250 nm to 190 nm. Molar ellipticity is shown on the *y*-axis. (**b**) Far-UV CD spectra of ANAC046 (172–338) and histidine–RCD1–RST(487–589) separately and of the interaction complex of ANAC046 (172–338) and histidine–RCD1–RST (487–589) mixed (1:1) and of predicted additive CD spectrum based on spectra of individual proteins (theoretical complex). Each protein (5 μM) was mixed in 10 mM Na_2HPO_4/NaH_2PO_4, pH 7.0. A total of 10 scans were averaged between 250 nm and 190 nm. (**c**) Far-UV CD spectrum of ANAC013 (161–498) and histidine–RCD1–RST(487–589) separately and of the interactions between ANAC013 (161–498) and RCD1–RST (499–572). Conditions as in (**b**). (**d**) Induced structural changes in the ANAC046 peptide ANAC046 (319–338) in 0 %–40 % (v/v) TFE analysed by far-UV CD. A total of eight scans were averaged of 25 μM ANAC046 (319–338) in 10 mM NaH_2PO_4/Na_2HPO_4, pH 7.0 and 10 % or 40 % TFE. The spectra were recorded at wavelength between 250 nm and 190 nm.

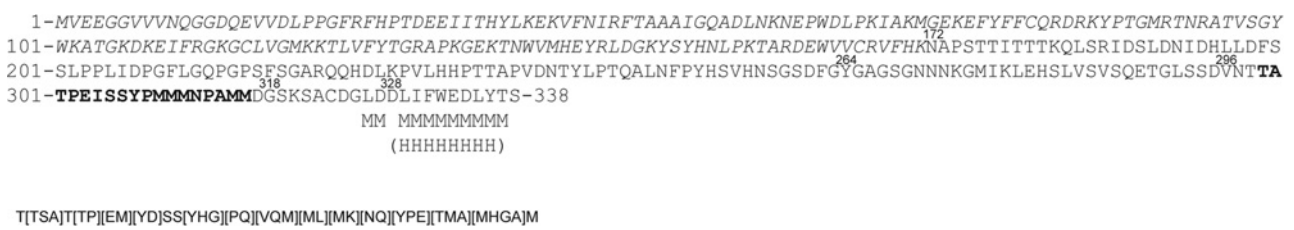

Figure 5 Amino acid sequence and structure analysis of ANAC046

Amino acid sequence of ANAC046. The NAC domain is shown in italics. The position of the predicted MoRF [41], α-helix [40] and MEME motif are shown by M and H below the sequence and by bold letters respectively. The MEME motif is also shown below the sequence. The position of residues forming the ends of the ANAC046 fragments and peptides analysed are marked above the sequence.

full-length ANAC046 and DBD–RCD1 (498–573) was relatively weak and only detectable by selective growth in the presence of adenine. To analyse whether intramolecular interactions between the NAC and the TRD domains of ANAC046 could hinder the interaction between the ANAC046 and RCD1, the ability of the two ANAC046 domains to interact was analysed. No interaction was detected when the two domains were physically split (Figure 7c). C-terminal truncations were also analysed for their ability to interact with DBD–RCD1 (498-573). This suggested that residues 205–299 of ANAC013 and that the very C-terminal MoRF region of ANAC046 were responsible for the interactions (Figures 7b–7c). Surprisingly, AD–ANAC046 (315–338), containing the MoRF region of ANAC046, did not interact with the RST domain. This may be due to steric hindrance from the GAL4 AD.

CD spectroscopy was subsequently used to analyse for structural changes occurring upon interaction between the RST domain and the NAC TRDs. The structure of the RST domain remains unknown. However, the far-UV CD spectrum of histidine–RCD1–RST (487–589) showed pronounced minima at 222 and 208 nm suggesting that the RST domain is dominated by α-helical structural elements (Figure 4b). A slight change of the absolute minimum towards a lower wavelength for the complex compared with the theoretical complex, obtained by adding the individual ANAC046 (172–338) and histidine–RCD1–RST (487–589) spectra, suggested that complex formation does not involve

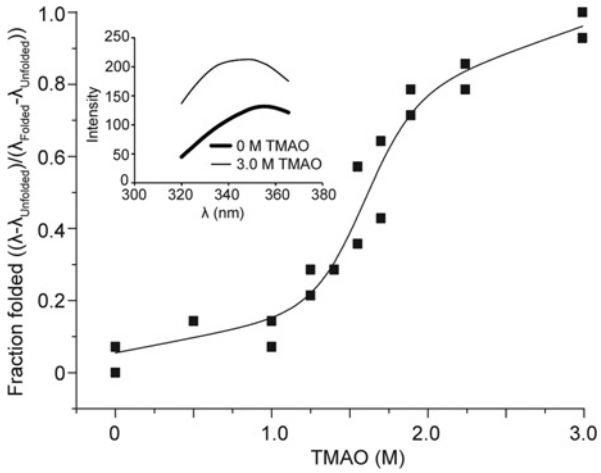

Figure 6 Induced folding of the ANAC046 TRD by TMAO

The normalized wavelengths of the fluorescence emission maxima of ANAC046 (172–338) plotted as a function of the TMAO concentration. The sigmoid curve observed was fitted to eqn (2) [48] to an $R^2 = 0.95$ yielding $\Delta G_{U\text{-}F} = 23.8$ kJ/mol $\pm$ 9.6 kJ/mol indicative of a two-state induction of folding by TMAO. The inset shows the scans from 320–370 nm of ANAC046 (172–338) in the presence and absence of 3 M TMAO, corrected for the contribution of buffers. The blue shift of the curve indicates that Trp^{332} is in a more hydrophobic environment when TMAO is present.

folding, but is suggestive of unfolding. Likewise, the CD spectrum of interacting ANAC013 (161–498) and histidine–RCD1–RST (487–589) showed a shift of the minimum around 200 nm towards a lower wavelength and also a decrease in the negativity at 222 nm compared with the theoretical complex suggestive of induced unfolding (Figure 4c). So, for both ANAC046 and ANAC013, complex formation with RCD1 did not result in induced folding.

Thermodynamics of RCD1–NAC TF interactions

ITC was used to analyse the thermodynamics of the interactions between the ANAC013 and ANAC046 TRDs and the RCD1 RST domain. This technique allows determination of the affinity of an interaction, in this study reported as the dissociation constant (K_d) and the change in enthalpy of binding (ΔH), whereas the change in Gibbs free energy (ΔG) and in entropy (ΔS), follows from these values [12]. The raw titration data displaying exothermic interactions were best fitted to the 'one set of sites' in the Origin ITC data analysis software. The affinities of the ANAC013 TRD, ANAC013 (161–498) and the ANAC046 TRD, ANAC046 (172–338), for the RST domain, RCD1–RST (499–572), was approximately the same with K_d values of 537 nM and 609 nM respectively (Figures 8a and 8b; Table 1). The RST domain contains one binding site for each NAC TRD identified by N values of 0.96 and 1.12 respectively (Table 1). Although there is only a minor difference in ΔG for the two interactions, the relative contributions of the changes in enthalpy and entropy were different. The change in entropy for binding of ANAC013 (161–498) to RCD1–RST (499–572) is relatively small and negative, indicating that binding is enthalpically driven. In contrast, the contributions from enthalpy and entropy to binding of ANAC046 (172–338) were of approximately the same size.

Since the ANAC046 TRD is simple with respect to putative interaction surfaces (Figure 1d), RCD1 binding to ANAC046 was mapped further. N-terminal truncation of ANAC046 (172–338) to generate ANAC046 (264–338) did not have a significant effect on binding (Table 1; Figure 5). By contrast and as expected from the yeast two-hybrid analysis (Figure 7c), C-terminal truncation generating ANAC046 (172–318) and ANAC046 (172–296) completely abolished binding. Binding to the synthetic peptides ANAC046 (319–338) and ANAC046 (328–338) was also analysed. Both span the MoRF region (Figure 5). ANAC046(328–338) represents a minimal region with α-helix and MoRF propensity, whereas ANAC (319–338) contains additional negatively-charged aspartic acids (Figures 8c–8d). Binding of these peptides to RCD1–RST (499–572) showed approximately the same K_d as was obtained for binding of ANAC046 (172–338) to RST. Interestingly, the relative contribution of ΔH and ΔS to binding was different, with a relatively smaller enthalpic contribution for the shortest peptide.

Since the RCD1-binding motif has been suggested to span one α-helix turn and contain both hydrophobic and acidic residues [24], the core of the ANAC046 RCD1-binding site was changed by single residue substitutions in ANAC046 (172–338). Changing Phe^{331} and Asp^{334} to alanine completely abolished binding when measured *in vitro* by ITC (Table 1). The same mutagenic changes in the corresponding GAL4 fusion proteins did not affect the ability to activate transcription in yeast (Figure 7d). However, they also abolished the ability to interact with the RST domain in yeast (Figure 7e). Whereas substitution of Glu^{333} with either alanine or proline did not significantly affect binding measured by ITC, the change of Trp^{332} into Pro decreased binding affinity. This may be explained both by a direct effect on binding and by an effect of α-helix propensity, since proline generally destabilizes α-helices. The implications in binding of Phe^{331} and Asp^{334}, separated by what corresponds to approximately one α-helix turn, supports the suggestion that the binding region forms an α-helix or a turn structure, at least in the complex.

The results indicated that hydrophobic Phe^{331} is essential for binding. However, changing negatively-charged Asp^{334} surprisingly also had a dramatic effect on binding, suggesting that ionic interactions are also essential for binding. The effect of the ionic strength on the interaction was therefore analysed. Although the affinity in the presence of 20 mM and 100 mM NaCl was similar, the presence of 500 mM NaCl obstructed binding (Table 1), reconfirming the significant role of ionic interactions. In conclusion, the very C-terminal region of ANAC046 is implicated in both transcriptional activity and interactions with the RST domain of RCD1. This interaction depends on both an aromatic, hydrophobic residue and an acidic residue in the ANAC046 TRD.

Induced structure in RCD1 interacting ANAC046 peptide

Since different secondary structure predictions did not agree with respect to the C-terminus of ANAC046 (results not shown), the ANAC046 (319–338) peptide was analysed by far-UV CD which suggested a highly unfolded peptide (Figure 4d) with an estimated α-helix content of 14 %. TFE can also be used to analyse secondary structure propensity and was used in this study to allow comparison with other similar studies [54]. Addition of TFE to 10 % (v/v) only marginally increased the estimated α-helical content to 18 %. By contrast, addition of TFE to 40 % markedly changed the CD spectrum. Thus, the global minimum was changed from 200 nm, typical of an unfolded state, to 222 nm and 208 nm, characteristic of α-helix and with an estimated α-helical content of 35 % (Figure 4d).

DISCUSSION

In this study, we show that the TRDs of six phylogenetic representative NAC TFs are all mostly disordered, but that their predicted order/disorder patterns differ (Figure 1d). The protein

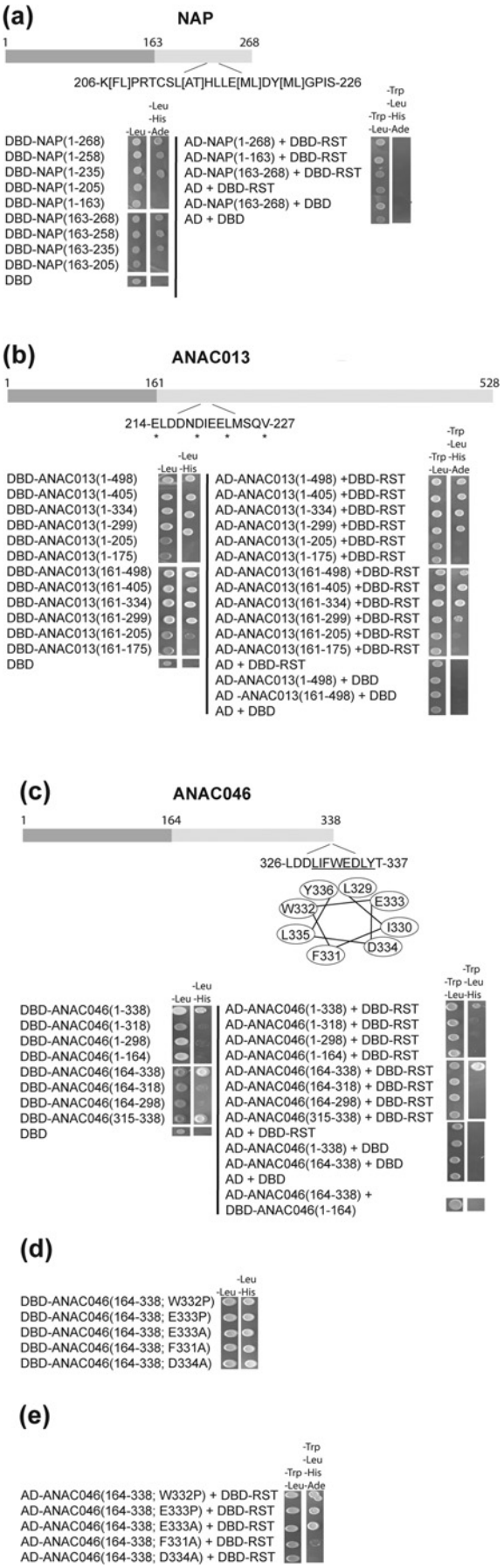

quartet model divides proteins into four conformational states [3,51]. Analysis by size-exclusion chromatography suggested that the average conformations of the ANAC046, NAP and ANAC019 TRDs correspond to pre-molten globules, whereas the ANAC013 TRD is more compact. The ensembles of NAC TRD conformations may in any case be better described as structural continuums [3,55]. CD analysis also suggested that the NAC TRDs are dominated by disorder, with an approximate α-helical content of around 20 %. For the ANAC046 TRD, this was surprising based on secondary structure predictions (Figure 1d), but in accordance with the ability to cooperatively induce structure in this TRD (Figure 6). Different MoRF patterns were also predicted for the NAC TRDs. In several cases, a MoRF coinciding with a predicted α-helix and/or a dip in the disorder profile represented a putative interaction determinant. For the ANAC046 TRD, the single MoRF region predicted was shown to be a functional hot spot responsible for both transcriptional activation and interaction with RCD1. Sequence features of ID regions are not easily transformed into protein function due to low complexity and poor conservation [3]. However, our *in silico* strategy is also useful for prediction of functional ID modules and can be used for example for identification of TF interaction partners. These are often identified using sensitive yeast two hybrid screenings. However, since TFs activate transcription in the yeast system (Figures 7a-c), TFs cannot be used as bait for such screenings. Use of short regions with high interaction potential as bait, such as the C-terminal NAP MoRF/α-helical region, would circumvent this problem.

The RCD1–TF system has been proposed as a model for studies of interactions between a folded hub protein and its disordered interactions partners [24]. In the present study, we contribute to the model by dissection of the RCD1–NAC interactions. The binding stoichiometry between RCD1 and ANAC013 or ANAC046 was one-to-one (Table 1), as determined by ITC analysis. Based on this and binding data for various ANAC046 fragments (Table 1), the presence of several non-continuous RCD1 binding sites in ANAC046 is unlikely. The 11 residues C-terminal peptide, ANAC046 (328–338), constitutes the smallest peptide shown to bind RCD1 and both Phe^{331} and Asp^{334} were essential for binding (Figure 7e and Table 1). Hydrophobic amino acid residues are enriched in linear motifs [6] and their contribution to binding may be mediated by the hydrophobic effect and by van der

Figure 7 Transcriptional activity and interactions of NAP, ANAC013 and ANAC046

(**a**) Top: domain structure of NAP with MEME sequence motif highlighted. Bottom, left of vertical bar: analysis of the ability of NAP to activate transcription in yeast. Fusions of GAL4 DBD and the indicated fragment of NAP were expressed in yeast and screened for their transactivation activity on the *HIS3* and *ADE2* reporter genes. Empty pDEST32 expressing GAL4 DBD served as negative control. Bottom, right of vertical bar: directed yeast two-hybrid assay for analysis of NAP and RCD1 interactions. Fusions of GAL4 DBD and the RST domain of RCD1 (residues 498–573; DBD–RST) and of GAL4 AD and the NAP fragment shown were expressed in yeast and screened for interactions through the ability to activate the reporter genes *HIS3* and *ADE2*. (**b**) Top: domain structure of ANAC013 with EDLL-like motif highlighted by stars. Bottom: as in (**a**) but for ANAC013. (**c**) Top: domain structure of ANAC046 with MoRF region highlighted as amino acid sequence and the predicted α-helix underlined and shown as α-helix wheel. Bottom: explanations as in (**a**) but for ANAC046, except that Ade was not used for selective growth in the protein interaction assays. (**d**) Fusions of GAL4 DBD and ANAC046 (164–338) with the indicated substitutions were expressed in yeast and screened for their transactivation activity on the *HIS3* and *ADE2* reporter genes. (**e**) Directed yeast two-hybrid assay for analysis of interactions between RCD1 and the indicated mutants of ANAC046 (164–338). Fusions of GAL4 DBD and the RST domain of RCD1 (residues 498–573; DBD–RST) and of GAL4 AD and the substituted ANAC046 (164–338) fragment shown were expressed in yeast and screened for interactions through the ability to activate the reporter genes *HIS3* and *ADE2*.

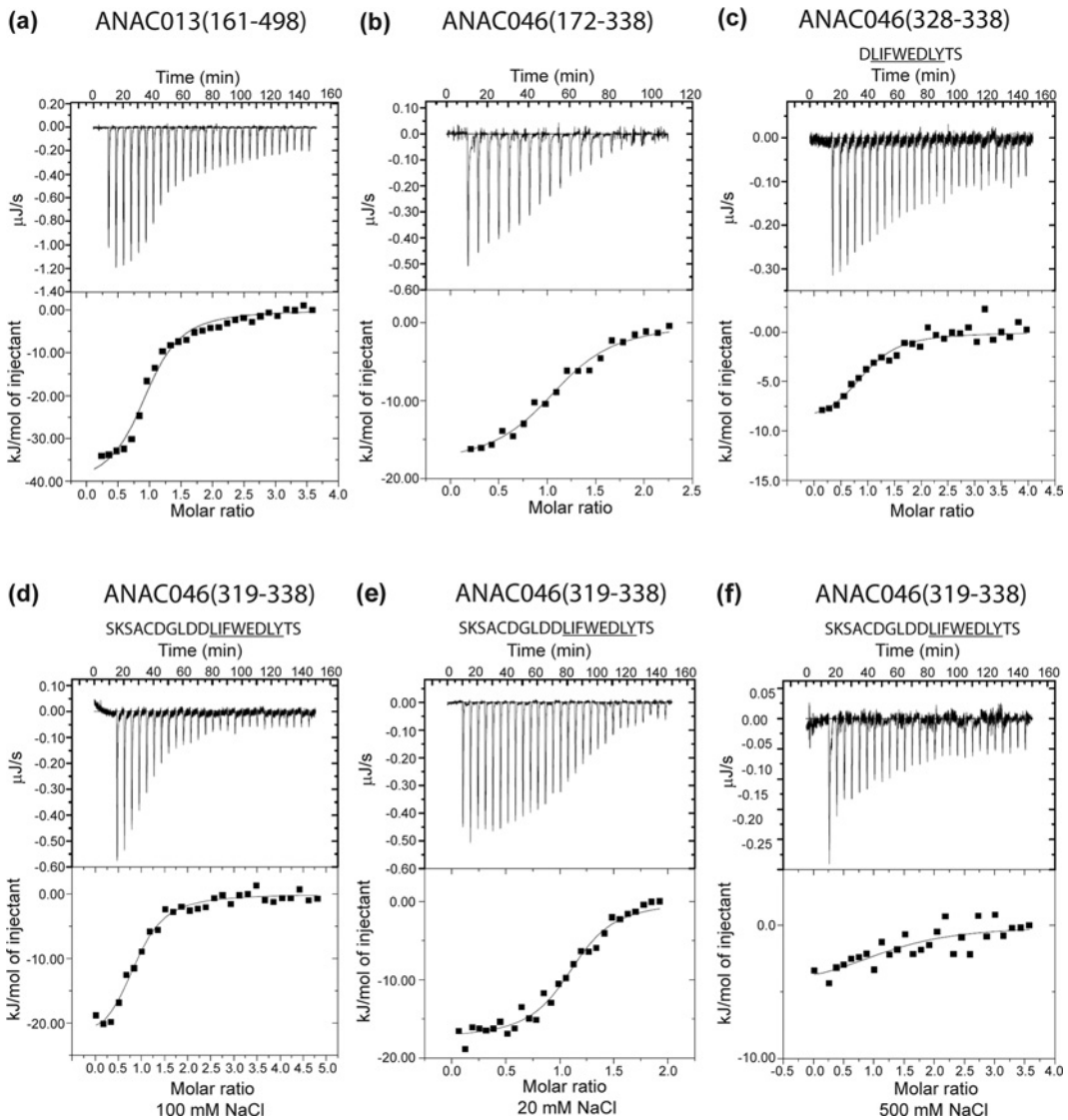

Figure 8 ITC measurements of the RCD1–RST–NAC interactions

ITC data showing the titration of RCD1–RST (499–572) into ANAC013 (161–498) (**a**); RCD1–RST (499–572) into ANAC046 (172–338) (**b**); RCD1–RST (499–572) into ANAC046 (328–338) (**c**); ANAC046 (319–338) into RCD1–RST(499–572) containing 100 mM NaCl (**d**); 20 mM NaCl (**e**); 500 mM NaCl (**f**). Experiments were performed as described in the Experimental section. In each panel, the upper portion shows baseline-corrected raw data from the titration and the lower portion shows the normalized integrated binding isotherm together with the fitted binding curve. Parameters from the fitted data points are presented in Table 1.

Walls interactions. Polycation–π interactions have also been implicated as driving forces for molecular recognition of IDPs (intrisically disordered proteins) [56] and cation–π (from Phe^{331}) forces may also contribute to the ANAC046–RCD1 complexes. However, abolishment of binding by changing an acidic residue or by increasing the ionic strength demonstrates that ionic interactions are also essential for binding at pH 7.4. The RST domain of RCD1 has a net positive charge (pI = 10.1) and may support ionic interactions with negatively-charged residues of the ANAC046 TRD (Figure 5). In accordance with this, a recent study suggested that electrostatic interactions are key components of interactions between ID regions and their partners [57]. So far, a common RCD1 target-binding site has not been identified [24,26]. However, similar chemical features of importance to the interaction are apparent for the DREB2a and ANAC046 peptides (Figure 9a). Thus, simultaneous substitution of Phe^{259} and Asp^{260} and of Glu^{263}, Leu^{264} and Leu^{265} of the DREB2a peptide abolished the ability to interact with RCD1 in yeast [26]. In conclusion, small peptides are sufficient for TF interactions with RCD1 and both hydrophobic and ionic interactions are essential. However, no common linear motif has been identified for RCD1-binding in the TFs. Lack of sequence similarity also characterizes the target peptides of the small hub protein CaM (calmodulin) [54,58].

Comparison of the RCD1 interaction network with the CaM interaction network is highly relevant. CaM is a small calcium-sensing hub protein which folds upon binding of Ca^{2+} and its binding to specific target sequences may induce α-helical structure in these [59]. CaM-binding peptides have different α-helical propensities ranging from α-helix before binding through folding-upon-binding to no detectable α-helix even in the presence of 40 % TFE [54,59]. CD analysis suggested that ANAC046 (319–338) is unstructured and not very prone to α-helix induction (Figure 4d) and that complex formation between the ANAC TRDs and the RST domain does not result in significant

Table 1 Thermodynamic parameters obtained from ITC analysis of ANAC013 or ANAC046 interactions with RCD

All experiments were performed as described in the Experimental section. Syringe/cell indicates whether RCD1–RST or NAC-protein is the titrant (in syringe) or the titrand (in cell). The standard errors for ΔH, K_d and N were obtained from Origin when fitting the data to a 'one set of sites' binding model.

Protein	[NaCl] (mM)	K_d (nM)	N†	ΔH (kJ/mol)	-TΔS (kJ/mol)	ΔG (kJ/mol)	Syringe/cell
ANAC013 (161–498)	100	537 ± 105	0.96 ± 0.03	− 41.0 ± 2.0	5.4	− 35.6	RCD1–RST (499–572)/NAC
ANAC046 (172–338)	100	609 ± 125	1.12 ± 0.03	− 18.3 ± 0.8	− 17.2	− 35.5	NAC/RCD1–RST (499–572)
ANAC046 (264–338)	100	699 ± 146	0.95 ± 0.03	− 18.0 ± 0.8	− 17.1	− 35.1	RCD1–RST (499–572)/NAC
ANAC046 (172–318)	100	NB*	NB*	NB*	NB*	NB*	NAC/RCD1–RST (499-572)
ANAC046 (172–296)	100	NB*	NB*	NB*	NB*	NB*	NAC/RCD1–RST (499–572)
ANAC046 (172–338; W332P)	100	3267 ± 980	0.81 ± 0.16	− 16.7 ± 4.2	− 14.6	− 31.3	NAC/RCD1–RST (499–572)
ANAC046 (172–338; E333P)	100	1000 ± 375	0.79 ± 0.09	− 18.4 ± 2.5	− 15.9	− 34.3	RCD1–RST (499–572)/NAC
ANAC046 (172–338; E333A)	100	917 ± 288	0.80 ± 0.08	− 18.0 ± 0.6	− 16.3	− 34.3	RCD1–RST (499–572)/NAC
ANAC046 (172–338; F331A)	100	NB*	NB*	NB*	NB*	NB*	RCD1–RST (499–572)/NAC
ANAC046 (172–338; D334A)	100	NB*	NB*	NB*	NB*	NB*	RCD1–RST (499–572)/NAC
ANAC046 (319–338)	100	609 ± 128	0.88 ± 0.04	− 23.8 ± 1.2	− 11.3	− 35.1	NAC/RCD1–RST (499–572)
ANAC046 (319–338)	20	320 ± 64	1.00 ± 0.02	− 17.1 ± 0.4	− 19.7	− 36.8	NAC/RCD1–RST (499–572)
ANAC046 (319–338)	500	NB*	NB*	NB*	NB*	NB*	NAC/RCD1–RST (499–572)
ANAC046 (328–338)	100	775 ± 335	0.95 ± 0.09	− 9.5 ± 1.2	− 25.3	− 34.8	NAC/RCD1–RST (499–572)

†N, molecular binding sites per mol protein.
*NB, no detectable binding.

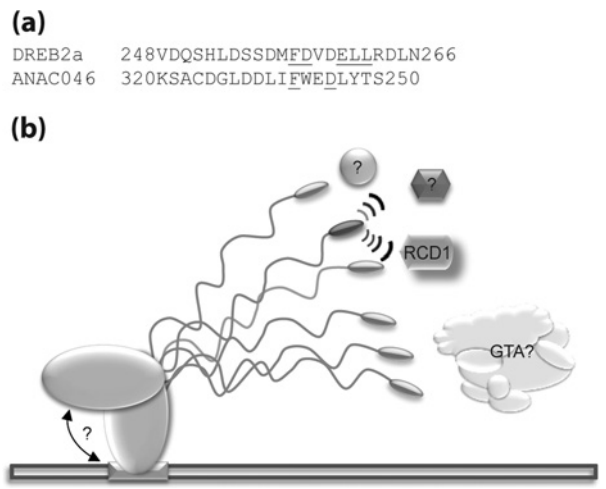

Figure 9 RCD1–TF interactions: determinants and entropic chain mechanism

(**a**) Sequence of DREB2a and ANAC046 RCD1 interacting peptides. Residues which together were shown to be essential for the interaction ability of DREB2a [26] are underlined and residues which were shown to be essential for ANAC046 interaction ability are underlined. (**b**) Schematic representation, not drawn to scale, of the interaction between ANAC046 and other proteins. The long entropic TRD chain of ANAC046 functions as a fishing rod with a C-terminal hot spot for interaction with, for example, the GTA (general transcriptional apparatus) and RCD1. The transparent tails of the TRD indicate fuzziness. It is unclear whether the identified hot spot executes its function when ANAC046 is bound to DNA or not. The figures marked with question-marks are potential interaction partners of the ANAC046 TRD.

structure induction (Figures 4b and 4c). The complex may involve fuzziness [15], as suggested for the *Hv*NAC013–*Hv*RCD1 complex [39], formation of a ι-MoRF without a regular pattern of backbone hydrogen bonds [6] or a turn-like structure. In support of this, insertion of α-helix-breaking proline at position 332 and 333 of ANAC046 did not completely abolish binding (Table 1). However, changing residues on the same side of a putative α-helix (Figure 7c) had similar effects. Thus, changing Phe^{331} and Asp^{334} on one-side-obstructed binding, whereas changing Glu^{333} or Trp^{332} on the other side to even proline had less severe effects on binding. Since an α-helix was unambiguously predicted for the RCD1-binding DREB2a peptide [24,26], the RCD1 binding site of the TFs may possess a range of propensities for α-helices or for different structures or be fuzzy. In addition, the RST domain of unknown tertiary structure may be malleable and able to adapt to different target structures. Further understanding of the RCD1–TF interactions awaits structural determination. In any case, if the RCD1-binding TF peptides are folded when bound, kinetic analysis will be needed to determine whether binding involves a pre-organized RCD1 binding site, folding-after-binding or a continuum of binding mechanisms [60].

The RCD1-binding TF peptides are either disordered in themselves, e.g. the ANAC046 peptide, or surrounded by disordered flanking regions, e.g. the DREB2a peptide [24,26]. The fact that N-terminal fusion of ANAC046 (315–338) to the GAL4 AD (Figure 7c) and of the DREB2a peptide to a structured protein [26] hindered interactions with RCD1 also suggests that flexibility of the RCD1-binding partner is needed. Having the binding region readily accessible within a disordered region may facilitate energetically favourable binding with ANAC046 as an extreme case (Figure 9b). Its long, disordered TRD constitutes a flexible fishing rod with a terminal bait for interactions with RCD1 and likely components of the basic transcriptional apparatus. Interestingly, TBP (TATA-box-binding protein)-associated factor 4, which is involved in assembly of the general TF complex TFIID (transcription factor II D), also contains an RST domain [61] and may be part of the ANAC046 interactome. ANAC046 represents a simple model for studies of ID function and mechanisms. NAC DBDs and TRDs may be separate functional modules [29] in contrast with, for example, the nuclear receptor TFs characterized by allosteric communication between separate functional domains [17]. Thus, the ANAC046 DBD and TRD did not functionally interact, at least when physically split (Figure 7c) and the DNA-binding specificity and affinity of senescence-associated ANAC092 was not affected by its TRD [62]. Future experiments will show whether the long ANAC046 TRD has functions in addition to being an entropic chain [3] optimized for catching interaction partners.

In this study, ITC was used to analyse the thermodynamics of the RCD1–NAC interactions. The binding energies of the small ANAC046 peptides for RCD1 ($\Delta G = -35.1$ kJ/mol and -34.8 kJ/mol respectively) are in the same range as the affinities of

the CaM-binding peptides for CaM ($\Delta G = -33$ kJ/mol to -47 kJ/mol), also determined by ITC [58,63]. The affinities of the small folded hub protein 14-3-3-ξ for target peptides derived from integrin tails were also obtained from ITC experiments and shown to be lower even when the peptides were phosphorylated ($\Delta G = -19.6$ kJ/mol to -30.9 kJ/mol) [64]. Tyr^{336} of ANAC046 or other residues of its RCD1-binding region may be subject to phosphorylation and thereby contribute to modulate binding. The thermodynamic parameters determined in this study also reveal aspects of the binding mechanisms. ANAC013 binding was driven by enthalpy (Table 1), as expected for binding involving ID regions [11] and could be explained by formation of novel hydrogen and ionic bonds. By contrast, and unexpectedly [11], binding of both the complete TRD of ANAC046 and N-terminal truncations thereof are driven by similar contributions from enthalpy and entropy. The entropic contribution could be the result of unfavourable dehydration of backbone polar groups and favourable dehydration of hydrophobic surfaces on ANAC046 and RCD1. The shorter peptides, ANAC046 (319–338) and ANAC046 (328–338) and the large ANAC046 TRD bound RCD1with similar affinities. Whereas the consensus 14-3-3-ξ-binding peptide was sufficient for high affinity binding to β2 integrin, additional residues outside the consensus regions were necessary for efficient binding of α4 integrin [64] and ID regions may wrap around binding partners [65]. On the basis of thermodynamics, a similar scenario seems unlikely for the ANAC046–RCD1 complex (Table 1). Interestingly, the relative contribution of enthalpy and entropy to binding changed upon peptide truncation (Table 1) and may represent enthalpy–entropy compensation. For ANAC046 (319–338) the enthalpic contribution was larger than the entropic contribution, but this pattern was reversed for the shortest peptide, ANAC046 (328–338). Speculating, removal of negatively-charged residues (Figures 8c and d) may decrease the enthalpic effect and removal of a flanking region which may become fixed upon complex formation makes the entropic contribution more favourable. In conclusion, the thermodynamic results obtained in the present study contribute to the understanding of the role of enthalpy and entropy in ID-based interactions and demonstrate the potential of ITC in studies of such interactions.

NAP, ANAC046 and ANAC013 were also analysed for their ability to activate transcription in yeast (Figures 7a–7c). The region responsible for this activity in NAP, NAP (205–235), contains a MEME motif (Figure 7a) which is conserved among NAP orthologues. Within the motif, L-X-X-L-L-E-M-D-Y is highly conserved and contains the φ-X-X-$\varphi\varphi$ consensus (φ: hydrophobic residue) and acidic residues, features that are characteristic of activation motifs [66]. However, additional mutational studies are required to identify specific residues of importance to the activity. The region 205–299 is responsible for transcriptional activation by ANAC013 and comprises a predicted α-helix coinciding with a E-D-L-L-like motif. The EDLL motif is found in a sub-group of AP2 TFs and functions as a strong activator of transcription [53] and the variant motif in ANAC013 may have a similar function. ANAC046 (315–338) contains the sequence D-D-L-I-F-W-E-D-L-Y-T-S which also resembles a typical acidic class activation domain with bulky hydrophobic amino acids embedded in an acidic matrix. In contrast with the interactions with RCD1, single residue mutations in the core F-W-E-D sequence were not sufficient to abolish the ability to activate transcription. This may be due to flexibility of the relevant interactions. Alternatively, the essential residues may be present outside the core MoRF region. Speculating, the function of RCD1 may be to repress a non-specific activation by binding to the activation domain of ANAC046. In conclusion, for all three NAC TFs, the region responsible for transcriptional activation has characteristics typical of known transcriptional activation motifs.

Great interest in the role of NAC TFs in senescence was initiated by the demonstration in 2006 [33] that replacement of a non-functional NAC allele in modern wheat with a functional ancestral counterpart resulted in increased wheat protein and iron content. ANAC046 and its closest barley homologue *Hv*NAC013 are both associated with senescence (Figures 1b–1c) [35,39] and based on its expression pattern *ANAC046* may be a convergence point for different signalling pathways relating to stress and senescence. Association of ANAC046 with a broad spectrum of physiological functions is in accordance with regulatory interactions with RCD1. RCD1 plays multiple roles in both stress and reactive oxygen species responses and the *rcd1* mutant plant displayed several pleiotrophic phenotypes, including senescence [27,28]. The regulatory potential of RCD1 was apparent from the demonstration that the RCD1-interaction-deficient *dreb2a* splice variant DREB2a.2 accumulates upon heat shock and senescence [26], suggesting that abrogation of the RCD1–DREB2A interaction is required for proper DREB2a level and function [26]. The importance of RCD1 interactions for function should be analysed for additional TFs of the RCD1 interactome [24]. Thus, the implication that ANAC013 is involved in oxidative stress responses [36] also makes this NAC TF a likely physiological interaction partner of RCD1. The present study contributes to the understanding of the ID-mediated interactions between TFs and RCD1 and reveals the complexity of the system. To further extend this understanding, future studies should involve a detailed calorimetric investigation of the binding of the many TF peptides to RCD1 in addition to atomic resolution structural studies. However, and most importantly, *in vitro* data on ID-based TF functionality should be translated to the *in vivo* organismal level [24]. This can be achieved by examining the complementation of *rcd1* and *tf* knockout mutants with RCD1 and TFs with altered interaction surfaces. ID is an obvious target for drugs modulating interactions with proof-of-concept from human diseases [67]. Such an approach could eventually be followed in plants to suppress or enhance TF function as a tool to dissect specific signalling pathways.

AUTHOR CONTRIBUTION

The planning of experiments and writing of the manuscript were mainly performed by Charlotte O'Shea and Karen Skriver with contributions from Mikael Kryger Jensen, Emil G. Palmkvist Stender, Birthe B. Kragelund and Martin Willemoës. Charlotte O'Shea performed most of the experimental characterization with contributions from Mikael Kryger Jensen and Emil G. Palmkvist Stender.

FUNDING

This work was supported by the Danish Agency for Science Technology and Innovation [grant number 274-07-0173)] to K.S.

REFERENCES

1 Dunker, A. K., Lawson, J. D., Brown, C. J., Williams, R. M., Romero, P., Oh, J. S., Oldfield, C. J., Campen, A. M., Ratliff, C. M., Hipps, K. W. et al. (2001) Intrinsically disordered protein. J. Mol. Graph Model **19**, 26–59 CrossRef PubMed

2 Tompa, P. (2012) Intrinsically disordered proteins: a 10-year recap. Trends Biochem. Sci. **37**, 509–516 CrossRef PubMed

3 van der Lee, R., Buljanm, M., Lang, B., Weatheritt, R. J., Daughdrill, G. W., Dunker, A. K., Fuxreiter, M., Gough, J., Gsponer, J., Jones, D. T. et al. (2014) Classification of intrinsically disordered regions and proteins. Chem. Rev. **114**, 6589–6631 CrossRef PubMed

4 Ward, J. J., Sodhi, J. S., McGuffin, L. J., Buxton, B. F. and Jones, D. T. (2004) Prediction and functional analysis of native disorder in proteins from the three kingdoms of life. J. Mol. Biol. **337**, 635–645 CrossRef PubMed

5 Dyson, H. J. and Wright, P. E. (2005) Intrinsically unstructured proteins and their functions. Nat. Rev. Mol. Cell Biol. **6**, 197–208 CrossRef PubMed
6 Vacic, V., Oldfield, C. J., Mohan, A., Radivojac, P., Cortese, M. S., Uversky, V. N. and Dunker, A. K. (2007) Characterization of molecular recognition features, MoRFs, and their binding partners. J. Proteome Res. **6**, 2351–2366 CrossRef PubMed
7 Fuxreiter, M., Simon, I., Friedrich, P. and Tompa, P. (2004) Preformed structural elements feature in partner recognition by intrinsically unstructured proteins. J. Mol. Biol. **338**, 1015–1026 CrossRef PubMed
8 Gould, C. M., Diella, F., Via, A., Puntervoll, P., Gemund, C., Chabanis-Davidson, S., Michael, S., Sayadi, A., Bryne, J. C., Chica, C. et al. (2010) ELM: the status of the 2010 eukaryotic linear motif resource. Nucleic Acids Res. **38**, D167–D180 CrossRef PubMed
9 Stein, A. and Aloy, P. (2008) Contextual specificity in peptide-mediated protein interactions. PLoS One **3**, e2524 CrossRef PubMed
10 Tompa, P., Fuxreiter, M., Oldfield, C. J., Simon, I., Dunker, A. K. and Uversky, V. N. (2009) Close encounters of the third kind: disordered domains and the interactions of proteins. Bioessays **31**, 328–335 CrossRef PubMed
11 Flock, T., Weatheritt, R. J., Latysheva, N. S. and Babu, M. M. (2014) Controlling entropy to tune the functions of intrinsically disordered regions. Curr. Opin. Struct. Biol. **26C**, 62–72 CrossRef
12 Ladbury, J. E. (2010) Calorimetry as a tool for understanding biomolecular interactions and an aid to drug design. Biochem. Soc. Trans. **38**, 888–893 CrossRef PubMed
13 Liu, J., Perumal, N. B., Oldfield, C. J., Su, E. W., Uversky, V. N. and Dunker, A. K. (2006) Intrinsic disorder in transcription factors. Biochemistry **45**, 6873–6888 CrossRef PubMed
14 Lee, C. W., Ferreon, J. C., Ferreon, A. C., Arai, M. and Wright, P. E. (2010) Graded enhancement of p53 binding to CREB-binding protein (CBP) by multisite phosphorylation. Proc. Natl. Acad. Sci. U.S.A. **107**, 19290–19295 CrossRef PubMed
15 Tompa, P. and Fuxreiter, M. (2008) Fuzzy complexes: polymorphism and structural disorder in protein-protein interactions. Trends Biochem. Sci. **33**, 2–8 CrossRef PubMed
16 Fuxreiter, M., Simon, I. and Bondos, S. (2011) Dynamic protein-DNA recognition: beyond what can be seen. Trends Biochem. Sci. **36**, 415–423 CrossRef PubMed
17 Hilser, V. J. and Thompson, E. B. (2011) Structural dynamics, intrinsic disorder, and allostery in nuclear receptors as transcription factors. J. Biol. Chem. **286**, 39675–39682 CrossRef PubMed
18 Ferreon, A. C., Ferreon, J. C., Wright, P. E. and Deniz, A. A. (2013) Modulation of allostery by protein intrinsic disorder. Nature **498**, 390–394 CrossRef PubMed
19 Hilser, V. J. (2013) Structural biology: signalling from disordered proteins. Nature **498**, 308–310 CrossRef PubMed
20 Pietrosemoli, N., Garcia-Martin, J. A., Solano, R. and Pazos, F. (2013) Genome-wide analysis of protein disorder in *Arabidopsis thaliana*: implications for plant environmental adaptation. PLoS One **8**, e55524 CrossRef PubMed
21 Marin, M. and Ott, T. (2014) Intrinsic disorder in plant proteins and phytopathogenic bacterial effectors. Chem. Rev. **114**, 6912–6932 CrossRef PubMed
22 Yoon, M. K., Shin, J., Choi, G. and Choi, B. S. (2006) Intrinsically unstructured N-terminal domain of bZIP transcription factor HY5. Proteins **65**, 856–866 CrossRef PubMed
23 Hardtke, C. S., Gohda, K., Osterlund, M. T., Oyama, T., Okada, K. and Deng, X. W. (2000) HY5 stability and activity in arabidopsis is regulated by phosphorylation in its COP1 binding domain. EMBO J. **19**, 4997–5006 CrossRef PubMed
24 Kragelund, B. B., Jensen, M. K. and Skriver, K. (2012) Order by disorder in plant signaling. Trends Plant Sci. **17**, 625–632 CrossRef PubMed
25 Blomberg, J., Aguilar, X., Brannstrom, K., Rautio, L., Olofsson, A., Wittung-Stafshede, P. and Bjorklund, S. (2012) Interactions between DNA, transcriptional regulator Dreb2a and the Med25 mediator subunit from *Arabidopsis thaliana* involve conformational changes. Nucleic Acids Res. **40**, 5938–5950 CrossRef PubMed
26 Vainonen, J. P., Jaspers, P., Wrzaczek, M., Lamminmäki, A., Reddy, R. A., Vaahtera, L., Brosché, M. and Kangasjärvi, J. (2012) RCD1-DREB2A interaction in leaf senescence and stress responses in *Arabidopsis thaliana*. Biochem. J. **442**, 573–581 CrossRef PubMed
27 Jaspers, P., Blomster, T., Brosche, M., Salojarvi, J., Ahlfors, R., Vainonen, J. P., Reddy, R. A., Immink, R., Angenent, G., Turck, F. et al. (2009) Unequally redundant RCD1 and SRO1 mediate stress and developmental responses and interact with transcription factors. Plant J. **60**, 268–279 CrossRef PubMed
28 Teotia, S. and Lamb, R. S. (2009) The paralogous genes radical-induced cell death1 and similar to RCD one1 have partially redundant functions during *Arabidopsis development*. Plant Physiol. **151**, 180–198 CrossRef PubMed
29 Jensen, M. K., Kjaersgaard, T., Nielsen, M. M., Galberg, P., Petersen, K., O'Shea, C. and Skriver, K. (2010) The *Arabidopsis thaliana* NAC transcription factor family: structure-function relationships and determinants of ANAC019 stress signalling. Biochem. J. **426**, 183–196 CrossRef PubMed
30 Olsen, A. N., Ernst, H. A., Leggio, L. L. and Skriver, K. (2005) NAC transcription factors: structurally distinct, functionally diverse. Trends Plant Sci. **10**, 79–87 CrossRef PubMed
31 Nakashima, K., Takasaki, H., Mizoi, J., Shinozaki, K. and Yamaguchi-Shinozaki, K. (2012) NAC transcription factors in plant abiotic stress responses. Biochim. Biophys. Acta **1819**, 97–103 CrossRef PubMed
32 Guo, Y. and Gan, S. (2006) AtNAP, a NAC family transcription factor, has an important role in leaf senescence. Plant J. **46**, 601–612 CrossRef PubMed
33 Uauy, C., Distelfeld, A., Fahima, T., Blechl, A. and Dubcovsky, J. (2006) A NAC gene regulating senescence improves grain protein, zinc, and iron content in wheat. Science **314**, 1298–1301 CrossRef PubMed
34 Hu, H., Da,i M., Yao, J., Xiao, B., Li, X., Zhang, Q. and Xiong, L. (2006) Overexpressing a NAM, ATAF, and CUC (NAC) transcription factor enhances drought resistance and salt tolerance in rice. Proc. Natl. Acad. Sci. U.S.A. **103**, 12987–12992 CrossRef PubMed
35 Breeze, E., Harrison, E., McHattie, S., Hughes, L., Hickman, R., Hill, C., Kiddle, S., Kim, Y. S., Penfold, C. A., Jenkins, D., Zhang, C. et al. (2011) High-resolution temporal profiling of transcripts during *Arabidopsis* leaf senescence reveals a distinct chronology of processes and regulation. Plant Cell **23**, 873–894 CrossRef PubMed
36 De, C. I., Vermeirssen, V., Van, A. O., Vandepoele, K., Murcha, M. W., Law, S. R., Inze, A., Ng, S., Ivanova, A., Rombaut, D., van de Cotte, B. et al. (2013) The membrane-bound NAC transcription factor ANAC013 functions in mitochondrial retrograde regulation of the oxidative stress response in *Arabidopsis*. Plant Cell **25**, 3472–3490 CrossRef PubMed
37 Ernst, H. A., Olsen, A. N., Skriver, K., Larsen, S. and Leggio, L. L. (2004) Structure of the conserved domain of ANAC, a member of the NAC family of transcription factors. EMBO Rep. **5**, 297–303 CrossRef PubMed
38 Chen, Q., Wang, Q., Xiong, L. and Lou, Z. (2011) A structural view of the conserved domain of rice stress-responsive NAC1. Protein Cell **2**, 55–63 CrossRef PubMed
39 Kjaersgaard, T., Jensen, M. K., Christiansen, M. W., Gregersen, P., Kragelund, B. B. and Skriver, K. (2001) Senescence-associated barley NAC (NAM, ATAF1,2, CUC) transcription factor interacts with radical-induced cell death 1 through a disordered regulatory domain. J. Biol. Chem. **286**, 35418–35429 CrossRef
40 Bryson, K., McGuffin, L. J., Marsden, R. L., Ward, J. J., Sodhi, J. S. and Jones, D. T. (2005) Protein structure prediction servers at University College London. Nucleic Acids Res. **33**, W36–W38 CrossRef PubMed
41 Disfani, F. M., Hsu, W. L., Mizianty, M. J., Oldfield, C. J., Xue, B., Dunker, A. K., Uversky, V. N. and Kurgan, L. (2012) MoRFpred, a computational tool for sequence-based prediction and characterization of short disorder-to-order transitioning binding regions in proteins. Bioinformatics **28**, i75–i83 CrossRef PubMed
42 Bailey, T. L., Williams, N., Misleh, C. and Li, W. W. (2006) MEME: discovering and analyzing DNA and protein sequence motifs. Nucleic Acids Res. **34**, W369–W373 CrossRef PubMed
43 Larkin, M. A., Blackshields, G., Brown, N. P., Chenna, R., McGettigan, P. A., McWilliam, H., Valentin, F., Wallace, I. M., Wilm, A., Lopez, R. et al. (2007) Clustal W and Clustal X version 2.0. Bioinformatics **23**, 2947–2948 CrossRef PubMed
44 Schmittgen, T. D. and Livak, K. J. (2008) Analyzing real-time PCR data by the comparative C(T) method. Nat. Protoc. **3**, 1101–1108 CrossRef PubMed
45 Uversky, V. N. (1993) Use of fast protein size-exclusion liquid chromatography to study the unfolding of proteins which denature through the molten globule. Biochemistry **32**, 13288–13298 CrossRef PubMed
46 Morrisett, J. D., David, J. S., Pownall, H. J. and Gotto, Jr, A. M. (1973) Interaction of an apolipoprotein (apoLP-alanine) with phosphatidylcholine. Biochemistry **12**, 1290–1299 CrossRef PubMed
47 Li, J., Motlagh, H. N., Chakuroff, C., Thompson, E. B. and Hilser, V. J. (2012) Thermodynamic dissection of the intrinsically disordered N-terminal domain of human glucocorticoid receptor. J. Biol. Chem. **287**, 26777–26787 CrossRef PubMed
48 Santoro, M. M. and Bolen, D. W. (1988) Unfolding free energy changes determined by the linear extrapolation method. 1. Unfolding of phenylmethanesulfonyl alpha-chymotrypsin using different denaturants. Biochemistry **27**, 8063–8068 CrossRef PubMed
49 Kim, S. G., Lee, A. K., Yoon, H. K. and Park, C. M. (2008) A membrane-bound NAC transcription factor NTL8 regulates gibberellic acid-mediated salt signaling in *Arabidopsis* seed germination. Plant J. **55**, 77–88 CrossRef PubMed
50 Yoshiyama, K., Conklin, P. A., Huefner, N. D. and Britt, A. B. (2009) Suppressor of gamma response 1 (SOG1) encodes a putative transcription factor governing multiple responses to DNA damage. Proc. Natl. Acad. Sci. U.S.A. **106**, 12843–12848 CrossRef PubMed
51 Uversky, V. N. (2002) What does it mean to be natively unfolded? Eur. J. Biochem. **269**, 2–12 CrossRef PubMed
52 Uversky, V. N. (2002) Natively unfolded proteins: a point where biology waits for physics. Protein Sci. **11**, 739–756 CrossRef PubMed
53 Tiwari, S. B., Belachew, A., Ma, S. F., Young, M., Ade, J., Shen, Y., Marion, C. M., Holtan, H. E., Bailey, A., Stone, J. K. et al. (2012) The EDLL motif: a potent plant transcriptional activation domain from AP2/ERF transcription factors. Plant J. **70**, 855–865 CrossRef PubMed
54 Dunlap, T. B., Kirk, J. M., Pena, E. A., Yoder, M. S. and Creamer, T. P. (2013) Thermodynamics of binding by calmodulin correlates with target peptide α-helical propensity. Proteins **81**, 607–612 CrossRef PubMed
55 Dyson, H. J. and Wright, PE. (1998) Equilibrium NMR studies of unfolded and partially folded proteins. Nat. Struct. Biol. **5** (Suppl), 499–503 CrossRef PubMed

56 Song, J., Ng, S. C., Tompa, P., Lee, K. A. and Chan, H. S. (2013) Polycation-π interactions are a driving force for molecular recognition by an intrinsically disordered oncoprotein family. PLoS Comput. Biol. **9**, e1003239 CrossRef PubMed
57 Wong, E. T., Na, D. and Gsponer, J. (2013) On the importance of polar interactions for complexes containing intrinsically disordered proteins. PLoS Comput. Biol. **9**, e1003192 CrossRef PubMed
58 Brokx, R. D., Lopez, M. M., Vogel, H. J. and Makhatadze, G. I. (2001) Energetics of target peptide binding by calmodulin reveals different modes of binding. J. Biol. Chem. **276**, 14083–14091 PubMed
59 Meador, W. E., Means, A. R. and Quiocho, F. A. (1992) Target enzyme recognition by calmodulin: 2.4 A structure of a calmodulin-peptide complex. Science **257**, 1251–1255 CrossRef PubMed
60 Kiefhaber, T., Bachmann, A. and Jensen, K. S. (2012) Dynamics and mechanisms of coupled protein folding and binding reactions. Curr. Opin. Struct. Biol. **22**, 21–29 CrossRef PubMed
61 Marr, M. T. (2009) TAF4 takes flight. Proc. Natl. Acad. Sci. U.S.A. **106**, 1295–1296 CrossRef PubMed
62 Lindemose, S., Jensen, M. K., de Velde, J. V., O'Shea, C., Heyndrickx, K. S., Workman, C. T., Vandepoele, K., Skriver, K. and Masi, F. D. (2014) A DNA-binding-site landscape and regulatory network analysis for NAC transcription factors in *Arabidopsis thaliana*. Nucleic Acids Res. **42**, 7681–7693 CrossRef PubMed
63 Wintrode, P. L. and Privalov, P. L. (1997) Energetics of target peptide recognition by calmodulin: a calorimetric study. J. Mol. Biol. **266**, 1050–1062 CrossRef PubMed
64 Bonet, R., Vakonakis, I. and Campbell, I. D. (2013) Characterization of 14–3-3-zeta Interactions with integrin tails. J. Mol. Biol. **425**, 3060–3072 CrossRef PubMed
65 Wang, Y., Fisher, J. C., Mathew, R., Ou, L., Otieno, S., Sublet, J., Xiao, L., Chen, J., Roussel, M. F. and Kriwacki, R. W. (2011) Intrinsic disorder mediates the diverse regulatory functions of the Cdk inhibitor p21. Nat. Chem. Biol. **7**, 214–221 CrossRef PubMed
66 Lee, C. W., Arai, M., Martinez-Yamout, M. A., Dyson, H. J. and Wright, P. E. (2009) Mapping the interactions of the p53 transactivation domain with the KIX domain of CBP. Biochemistry **48**, 2115–2124 CrossRef PubMed
67 Oldfield, C. J., Meng, J., Yang, J. Y., Yang, M. Q., Uversky, V. N. and Dunker, A. K. (2008) Flexible nets: disorder and induced fit in the associations of p53 and 14-3-3 with their partners. BMC Genomics **9** (Suppl 1), S1 CrossRef

Received 12 August 2014/24 October 2014; accepted 28 October 2014
Published as BJ Immediate Publication 28 October 2014, doi:10.1042/BJ20141045